Report

www.the-innovation.org

Mechanism of progressive broad deformation from oceanic transform valley to off-transform faulting and rifting

Fan Zhang,[1,3] Jian Lin,[1,2,3,4,*] Zhiyuan Zhou,[2] Hongfeng Yang,[5] and Jason P. Morgan[2]

*Correspondence: jlin@whoi.edu

Received: April 22, 2021; Accepted: November 26, 2021; Published Online: November 27, 2021; https://doi.org/10.1016/j.xinn.2021.100193

GRAPHICAL ABSTRACT

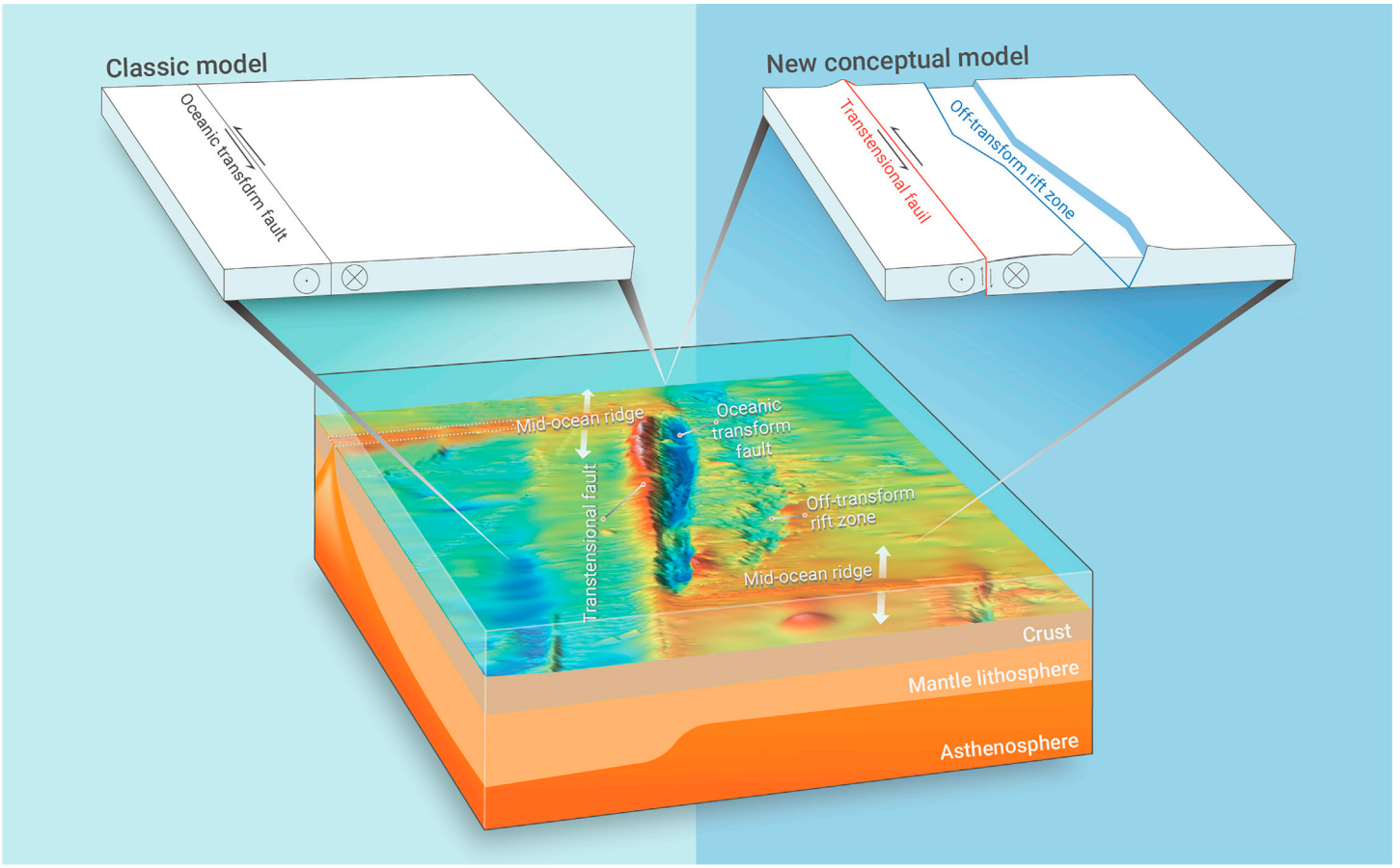

PUBLIC SUMMARY

- Systematic progression of complex deformation near transform faults is revealed
- Progressive complex broad deformation is an inherent feature of oceanic transform faults
- TTFs on transform wall and off-transform rifting formed in response to plate rotation
- Off-transform rift zones can develop into new transform plate boundaries

Report

Mechanism of progressive broad deformation from oceanic transform valley to off-transform faulting and rifting

Fan Zhang,[1,3] Jian Lin,[1,2,3,4,*] Zhiyuan Zhou,[2] Hongfeng Yang,[5] and Jason P. Morgan[2]

[1]Key Laboratory of Ocean and Marginal Sea Geology, South China Sea Institute of Oceanology, Innovation Academy of South China Sea Ecology and Environmental Engineering, Chinese Academy of Sciences, Guangzhou 510301, China

[2]Department of Ocean Science and Engineering, Southern University of Science and Technology, Shenzhen 518055, China

[3]Southern Marine Science and Engineering Guangdong Laboratory (Guangzhou), Guangzhou 511458, China

[4]Department of Geology and Geophysics, Woods Hole Oceanographic Institution, Woods Hole, MA 02543, USA

[5]Earth System Science Programme, The Chinese University of Hong Kong, Shatin, Hong Kong 999077, China

*Correspondence: jlin@whoi.edu

Received: April 22, 2021; Accepted: November 26, 2021; Published Online: November 27, 2021; https://doi.org/10.1016/j.xinn.2021.100193

Citation: Zhang F., Lin J., Zhou Z., et al., (2022). Mechanism of progressive broad deformation from oceanic transform valley to off-transform faulting and rifting. The Innovation **3(1)**, 100193.

Oceanic transform faults (TFs) are commonly viewed as single, narrow strike-slip seismic faults that offset two mid-ocean ridge segments. However, broad zones of complex deformation are ubiquitous at TFs. Here, we propose a new conceptual model for the progressive deformation within broad zones at oceanic TFs through detailed morphological, seismic, and stress analyses. We argue that, under across-transform extension due to a change in plate motion, plate deformation occurs first along high-angle transtensional faults (TTFs) within the transform valleys. Off-transform normal faults (ONFs) form when across-transform deviatoric extensional stresses exceed the yield strength of the adjacent oceanic lithosphere. With further extension, these normal faults can develop into off-transform rift zones (ORZs), some of which can further develop into transform plate boundaries. We illustrate that such progressive complex deformation is an inherent feature of oceanic TFs. The new conceptual model provides a unifying theory to explain the observed broad deformation at global transform systems.

INTRODUCTION

In a simplified steady-state view, a single, narrow strike-slip fault would be sufficient to accommodate the differential motion between the two adjacent mid-ocean ridge segments. In reality, spreading centers frequently experience minor changes in plate motion, changes that can lead to extension or compression along transform plate boundaries.[1–6] These ubiquitous changes in relative plate motion and their induced deformation along and around transform faults (TFs) should be considered to be fundamental processes along ridge-transform systems.

Striking examples of broad transform zones are seen along the Pacific-Antarctic Ridge (PAR), which separates the Pacific and Antarctic plates (Figure 1), which formed ~68 mya.[7] The spreading direction along the PAR has been gradually changing in a clockwise rotation since ~12 Ma, with an abrupt change occurring at ~5.9 Ma.[8] The significant changes in the direction of plate motion, diverse spreading rates, and diverse transform offset lengths along the PAR make it an ideal laboratory to study transform dynamics. The Heezen, Tharp, and Pitman TFs, located at ~54°S, 56°S, and 65°S along the PAR, have full slip rates of 78.9, 79.0, and 54.0 mm/year,[9–11] and mega to moderate transform offset lengths of 390, 460, and 80 km (Figure 1), respectively. Since these three transform systems are located close to the Euler pole for relative motion between the Pacific and the Antarctic plates, their morphology is especially sensitive to small changes in relative plate motion.[12,13]

In comparison to most transform systems,[14,15] the Heezen and Tharp TFs are associated with unusually deep transform valleys. The depth difference between the crest of the transform wall uplift and the bottom of the transform valley locally reaches more than 5 km within an across-transform distance of only ~20 km (Figures 1 and S1–S3). Prominent narrow uplifts are found to extend hundreds of kilometers parallel to the strike of the TFs. Furthermore, off-transform rift zones (ORZs) are observed at distances of ~30–40 km sub-parallel to the active TFs (Figure 1). The shorter Pitman TF shows a morphological anomaly similar to those of the Heezen and Tharp TFs, but with smaller amplitudes (Figures 1, S2, and S3A). Previous studies have proposed multiple mechanisms for the observed uplift and the exceptionally deep transform valleys[7] in the Heezen and Tharp systems: (1) thermal and viscodynamic forces near the ridge-transform intersection, (2) combination of a flexural response to the negative load of the adjacent valleys, (3) mantle serpentinization, (4) heating by mid-transform spreading axes, or (5) extension or compression across the TF.[16–19] However, the mechanism for the formation and evolution of their neighboring intraplate off-transform normal faults (ONFs) and ORZs, as well as their relationship with the deformation within the transform valley, remain elusive.

Here, we use the morphology, vertical deformation, and seismicity of the Heezen, Tharp, and Pitman transform systems to illustrate the specific mechanisms

Table 1. Topographic features of transtensional faults and earthquake focal mechanisms

	Heezen	Tharp	Pitman
Length (km)	390	464	80
Age offset (Ma)	12	16	3
Width (km)			
Valleys	10.1–16.2	8.1–28.9	6.0–6.7
Uplifts	13.4–16.3	7.9–22.7	11.6–11.9
Depth (km)			
Valleys	1.1–2.4	0.4–2.3	0.6–0.7
Uplifts	0.2–2.2	0.3–2.5	0.7–0.8
Area (km^2)			
Valleys	8.2–19.5	1.5–29.2	2.0–2.5
Uplifts	1.5–17.6	1.2–21.4	4.2–4.7
Mean strike (°)			
Strike slip	160.1	156.3	
Normal	98.4	95.5	
Mean dip (°)			
Strike slip	75.5	75.6	
Normal	46.9	46.5	
Number			
Strike slip	93	137	
Normal	8	6	
Magnitude			
Strike slip	4.8–6.4	4.8–6.6	
Normal	5.0–6.7	5.1–6.1	
Moment (dyne cm)			
Strike slip	5.45×10^{26}	5.63×10^{26}	
Normal	1.61×10^{26}	2.66×10^{25}	

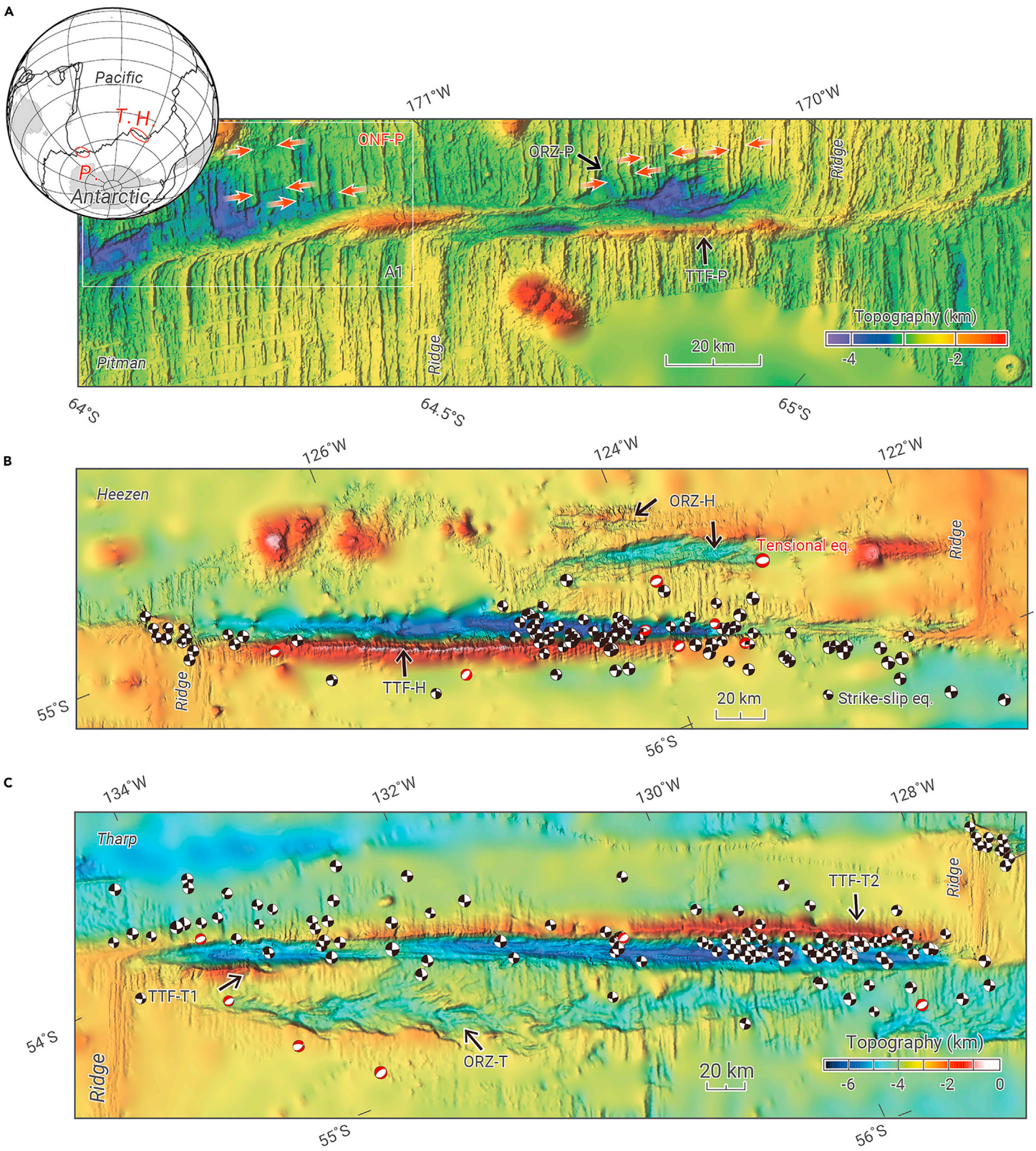

Figure 1. Topography and earthquakes at Pitman, Heezen, and Tharp transform faults (A–C) Topography of the Pitman (A), Heezen (B), and Tharp (C) transform faults (TFs). P., H., and T. represent the Pitman, Heezen, and Tharp transform faults, respectively. TTF-P, TTF-H, TTF-T1, and TTF-T2 are transform-transtensional faults (TTFs) observed at the Pitman, Heezen, and Tharp transform fault segments 1 and 2, respectively. ORZ-P, ORZ-H, and ORZ-T are off-transform rift zones (ORZs) observed at the Pitman, Heezen, and Tharp transform faults, respectively. Focal mechanisms of relocated earthquakes along the Heezen and Tharp TFs are from Sykes and Ekstrom (2012).[27]

that underlie the complex tectonics of their adjacent zones with widespread deformation. We show that the initiation of these ONFs and the ORZs appears to take place when across-transform extensive stresses exceed the level required to break their adjacent oceanic lithosphere. We further propose that some ORZs develop into future new TFs oblique to the original transform. Through additional discussion of deformation at exemplar TFs along the fast-, slow-, and ultra-slow-spreading East Pacific Rise (EPR), Mid-Atlantic Ridge (MAR), Southwest Indian Ridge (SWIR), and Southeast Indian Ridge (SEIR), we demonstrate that this mode of deformation within a broad zone is an inherent feature of near-transform oceanic crust.

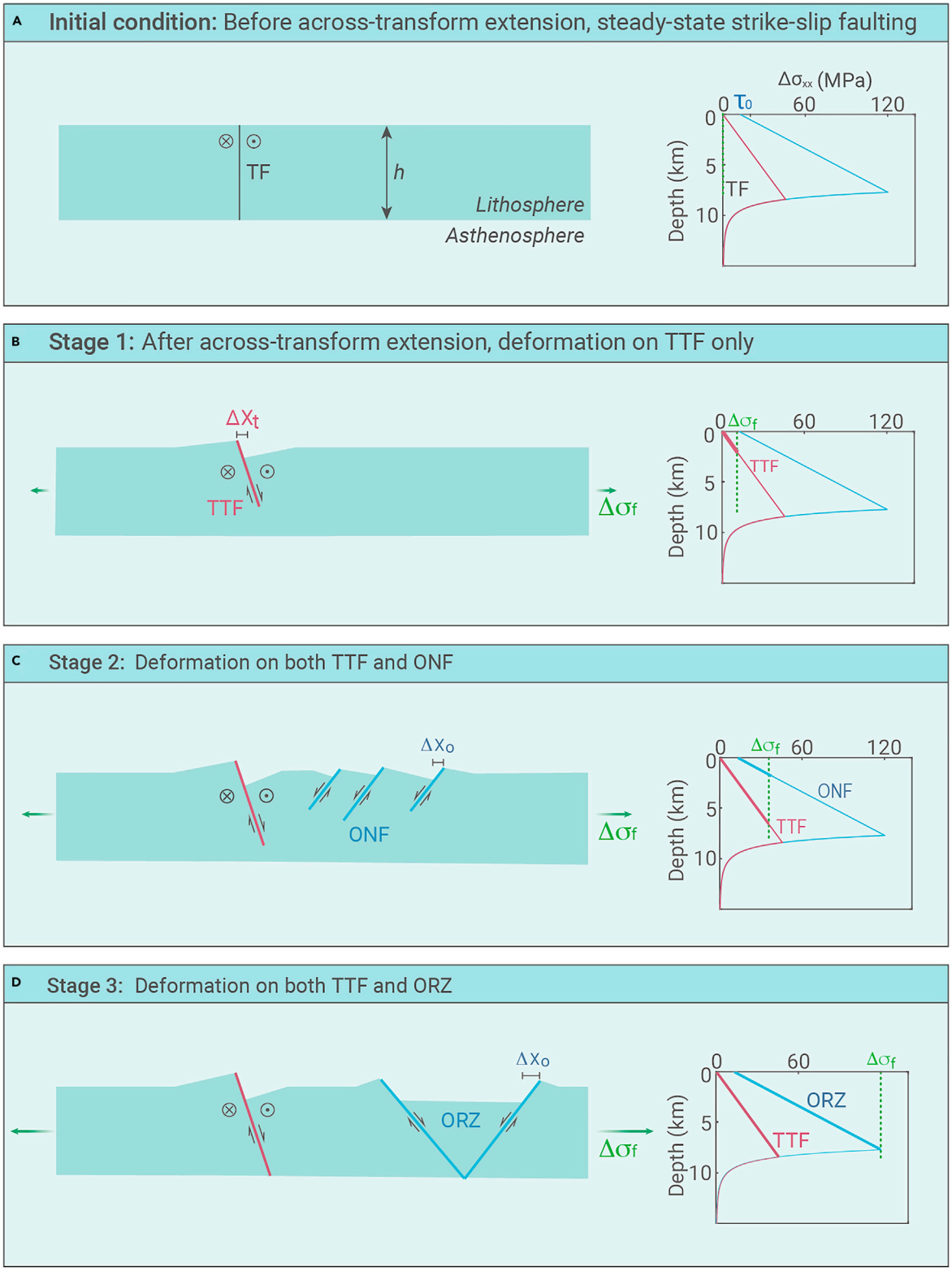

Figure 2. Stress analysis of the formation of transform-transtensional fault, off-transform normal fault, and off-transform rift zone. $\Delta\sigma_f$ is the horizontal extensional stress caused by plate rotation. (A) Cross section and stress of a steady-state TF. (B) Formation of a TTF with a high dip angle. (C) ONF forms when extension continues, which co-exists with the TTF. (D) When extension further increases, an ORZ forms when a pair of conjugate ONFs cuts through the entire plate.

RESULTS

Deformation and earthquake focal mechanisms of TTF versus ORZ

The Heezen and Tharp TFs share similar abnormal morphological features (Figures 1B, 1C, and S1–S3) that include prominent transform-parallel uplifts and deep TF valleys (see details in supplemental information). The transform valleys and transform uplifts of the Heezen and Tharp systems are similar in their depths, widths, and cross-sectional areas, with differences of only 8%–29% (Table 1). Analytical modeling suggests that these observed similarities in their morphological features are more consistent with these transtensional faults (TTFs) being produced by deformation along a single high-angle extensional normal fault as opposed to compressional thrust faulting, for which the amplitude of uplift would be predicted to be significantly greater than the amplitude of valley.[20] The observed surface fault throws (Δy_t) at TTF-H along the Heezen, TTF-T1 and TTF-T2 along the Tharp, and TTF-P along the Pitman

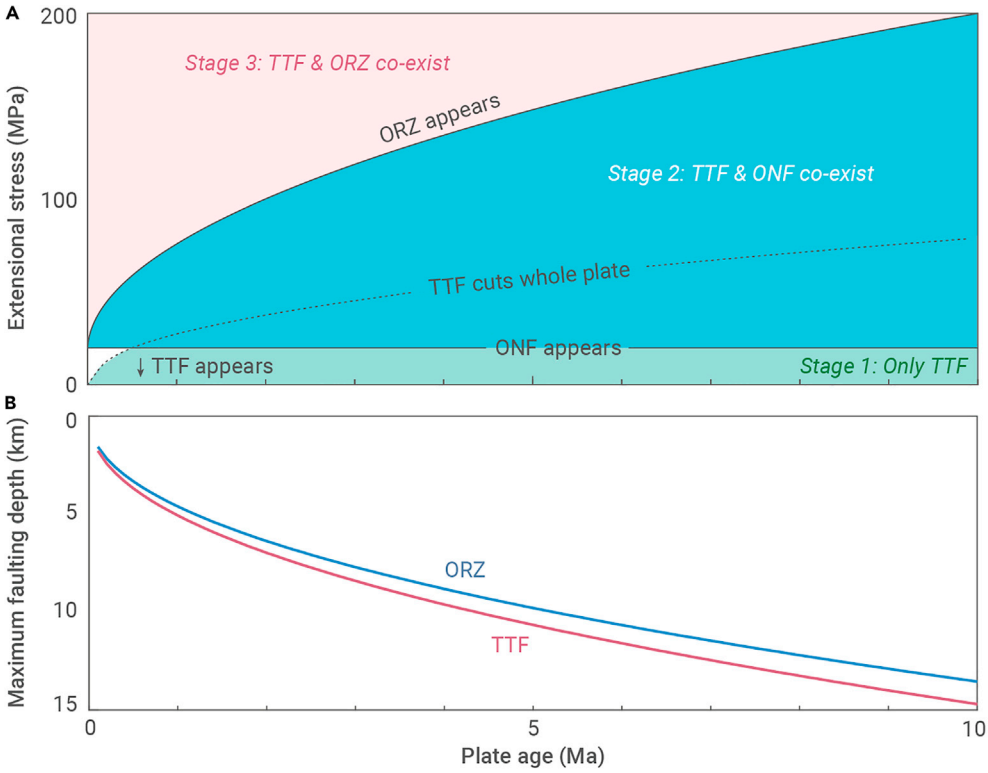

Figure 3. Calculated extensional stress and maximum faulting depth as a function of plate age
(A) Required deviatoric extensional stress for generating a TTF, ONF, and ORZ as a function of plate age. As deviatoric extensional stress increases, a TTF first appears, an ONF forms next, then a TTF cuts the whole plate at the TF, and finally, the ORZ-bounding faults cut through the entire off-transform plate. (B) Calculated maximum faulting depth of TTF and ORZ as a function of plate age.

are measured to be 3.7 ± 1.2, 2.8 ± 1.1, 3.4 ± 1.0, and 1.4 ± 0.4 km, respectively (Figures S2 and S3), significantly larger than the global average of the depth difference between a transform valley and its adjacent crust for intermediate spreading systems.[14,15] These features imply the presence of "excess" vertical tectonic deformation. The accumulated surface fault heaves (Δx_t) (see details in supplemental information, Figure S1) of TTF-H, TTF-T1, TTF-T2, and TTF-P are estimated to be 9.6 ± 2.5, 8.5 ± 1.9, 11.2 ± 2.8, and 4.2 ± 1.4 km, respectively (Figure S3). We interpret these result to mean that the TTFs form at high-angle TFs that otherwise experience predominantly strike-slip motion.[21–23]

Transform-sub-parallel ORZ-H and ORZ-T are observed at distances of 30–40 km from the Heezen and Tharp TFs, whereas ORT-P is observed at distances of 0–10 km from the Pitman TF. The accumulated surface throws (Δy_t) along ORZ-H, ORZ-T, and ORZ-P are 1.2 ± 0.4, 0.7 ± 0.4, and 0.4 ± 0.3 km, respectively (Figure S4). The accumulated surface heaves (Δx_t) (see details in supplemental information, Figure S1) of ORZ-H, ORZ-T, and ORZ-P are 11.2 ± 2.0, 11.7 ± 5.7, and 5.1 ± 1.2 km, respectively (Figure S1). Although the surface fault throw of each TTF is about three to four times that of its corresponding ORZ, the surface fault heaves of the TTFs are similar to those of the ORZs (Figure S3), indicating that the extensional strains released by the TTFs and ORZs are of the same order of magnitude. We infer that across-transform extensional strains are linked to the recent clockwise plate rotation along the PAR system.[24,25]

The transtensional strains indicated by these morphological features are further supported by focal mechanism solutions of relocated earthquakes along the Heezen and Tharp systems.[25,26] For magnitude ≥ 4.8 relocated earthquakes within the Heezen and Tharp systems from 1976 to 2020,[26,27] the accumulated seismic moment of the normal component is 1.88×10^{26} dyne cm, which is ~17% of the strike-slip moment (11.08×10^{26} dyne cm; Table 1). This indicates that transform shearing remains the dominant mode of strain release within these systems. The average dip angles of the transtensional earthquakes (−45° < rake < 0°) at the Heezen and Tharp TFs are 75.5° ± 14.3° and 75.6° ± 12.1°, respectively (black beachballs in Figures 1B and 1C and Table 1). In contrast, focal mechanism solutions show that only predominantly normal fault earthquakes (−135° < rake < −45°) occurred at the ORZs of the Heezen and Tharp systems from 1976 to 2020[26,27] (red beachballs in Figures 1B and 1C and Table 1), indicating that the ORZs are undergoing active extensional deformation. The average dip angles of the normal faulting earthquakes in the ORZs of the Heezen and Tharp systems are 46.9° ± 15.2° and 46.5° ± 9.4°, respectively (Table 1). Strikes of the normal faulting events in the Heezen and Tharp ORZs are also consistent with the overall strikes of the predominant seafloor abyssal fabrics in these ORZs.

Mechanisms of sequential plate deformation in response to plate rotation

A mechanical analysis reveals that the extensional strain in response to a local change in plate rotation should be initially accommodated by normal faulting along steeply dipping faults within the transform valley[28] (stage 1; Figure 2B). However, if local deviatoric extensional stresses continue to rise, then ONFs can start to form in adjacent crust when local stresses exceed the local rock cohesion (stage 2; Figure 2C). We hypothesize that some of the ONFs cut through the entire lithospheric plate to become ORZ-bounding faults with moderate dip angles (stage 3; Figure 2D). The maximum faulting depth of both TTF and ORZ increases with plate age, whereas the modeled depth for TTF is slightly greater than that for ORZ (Figure 3B). The partition of deformation between a TTF and its neighboring ORZ depends on the apparent friction coefficient along the TTF plane. If the friction on the TTF is relatively small,[28–30] i.e., $\mu_t \approx 0.1$, the following could occur in response to increasing deviatoric extensional stresses: (1) the TTF deforms initially; (2) deformation then occurs along both the TTF and the ONF; and finally, (3) the ORZ forms (Figure 3A). The observed co-existence of deformation along both the TTF and its adjacent ORZ (Figures S2B and S2D) support the above mechanistic model.

In summary, the tectonic events occur progressively from the oceanic TF valley to off-transform faulting and rifting (Figure 4). A local change in the direction of plate motion induces deviatoric extensional stresses across the TF. At first, the lithosphere adjacent to the TF undergoes near-vertical deformation on its pre-existing steeply dipping TTF (stage 1; Figures 2B and 4B). As local deviatoric extensional stresses increase in response to the local change in plate motion, they eventually exceed the rock's cohesive strength. At this point, the adjacent plate breaks to form new ONFs (stage 2; Figures 2C and 4C). Some ONFs will continue to deform, evolving into an ORZ of the rift-bounding faults with low to moderate dip angles (stage 3; Figure 4D). Evidence from seafloor morphology and active earthquake focal mechanisms shows that the TTFs and ONF/ORZs can remain simultaneously active.

DISCUSSION

The ubiquitous broad deformation zones of global transform systems

Complex deformation within a broad plate deformation zone appears to be an inherent feature of many oceanic TFs. This is further illustrated by the following additional distinctive examples[1,4,5,12,18,31–36] (Figure 5): (1) TTFs and ORZs on both sides of the Udintsev TF on the PAR[12] (Figure 5A); (2) a TTF and normal faults that cut a dome-shaped uplift zone along the Atlantis II TF on the MAR[29] (Figure 5B); (3) formation of a TTF and reactivation of the adjacent fracture zone at the Vema TF on the MAR[1,32–34] (Figure 5C); (4) development of intratransform spreading centers (ITSCs) at the Siqueiros TF on the EPR[35] (Figure 5D); (5) formation of En-echelon faults in a transform relay zone of overlapping basins at the Andrew Bain TF on the SWIR[36] (Figure 5E); (6) mantle uplift and exhumation at the St. Paul TF on the MAR[4] (Figure 5F); (7) TTF and ONF at ~128°E on the SEIR (Figures S3B–S3E); and (8) formation of Easter, Juan Fernandez, and Galapagos microplates on the EPR.[37–40]

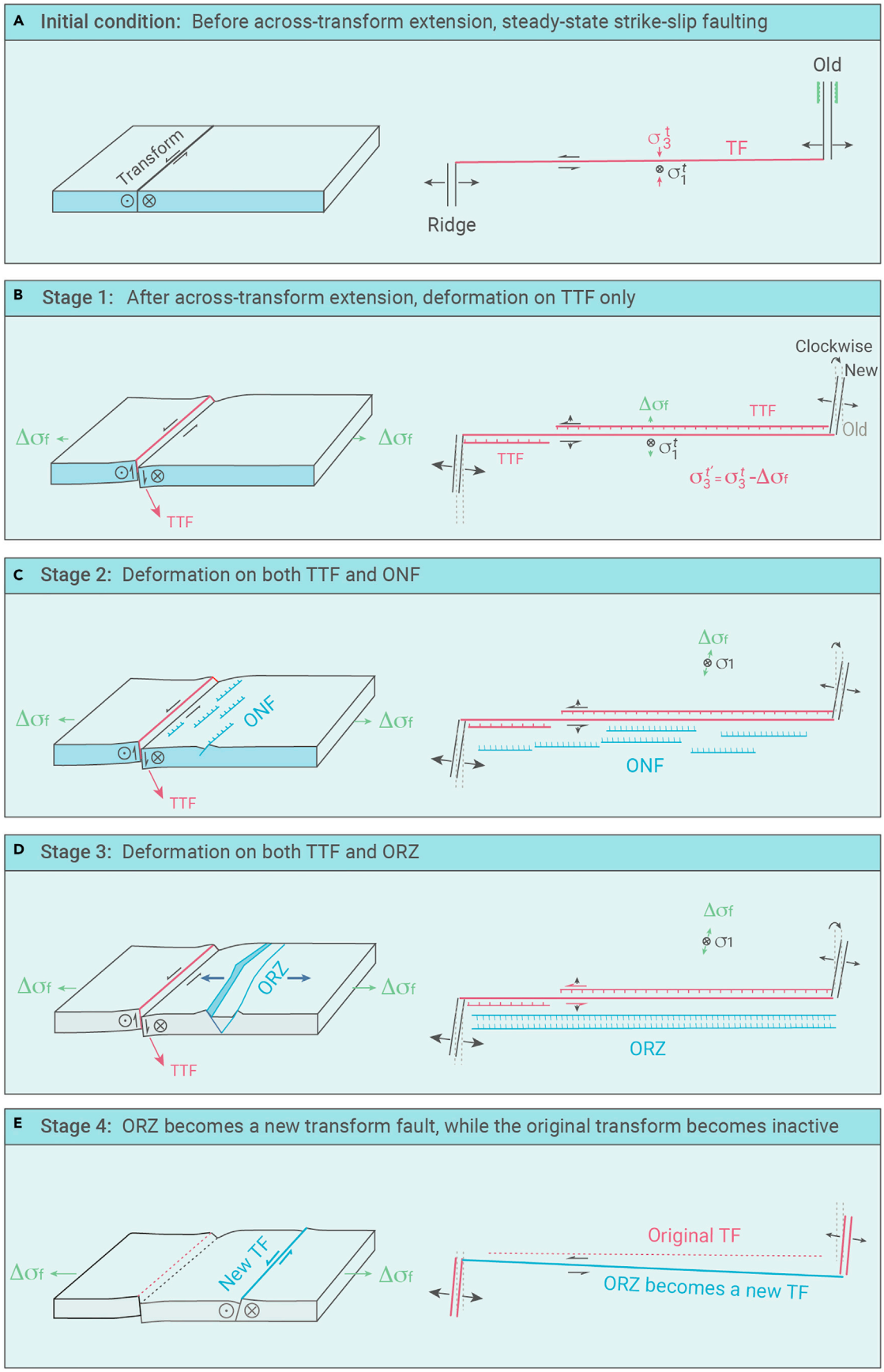

Figure 4. Tectonic responses of a mega TF to a change in relative plate motion that induces local plate rotation σ_1 is the maximum principal stress of the ONF/ORZ. σ_1^t and σ_3^t are the maximum and minimum principal stress of the TF before rotation, while $\sigma_1^{t'}$ and $\sigma_3^{t'}$ are the maximum and minimum principal stress of the TF after plate rotation. $\Delta\sigma_f$ is the horizontal extensional stress caused by plate rotation. (A) A steady-state ridge-transform system before the local plate rotation. (B) Formation of a TTF along the TF after an increment of plate rotation. Gray dashed double line marks the old ridge axis. (C) Formation of ONFs sub-parallel to the TF. (D) When the deviatoric extensional stress becomes large enough to break the entire plate, a pair of conjugate ONFs develops into an ORZ. (E) Finally, the ORZ develops into a new TF to accommodate the new spreading direction. The old transform fault becomes inactive (dashed lines), and a new ORZ can form.

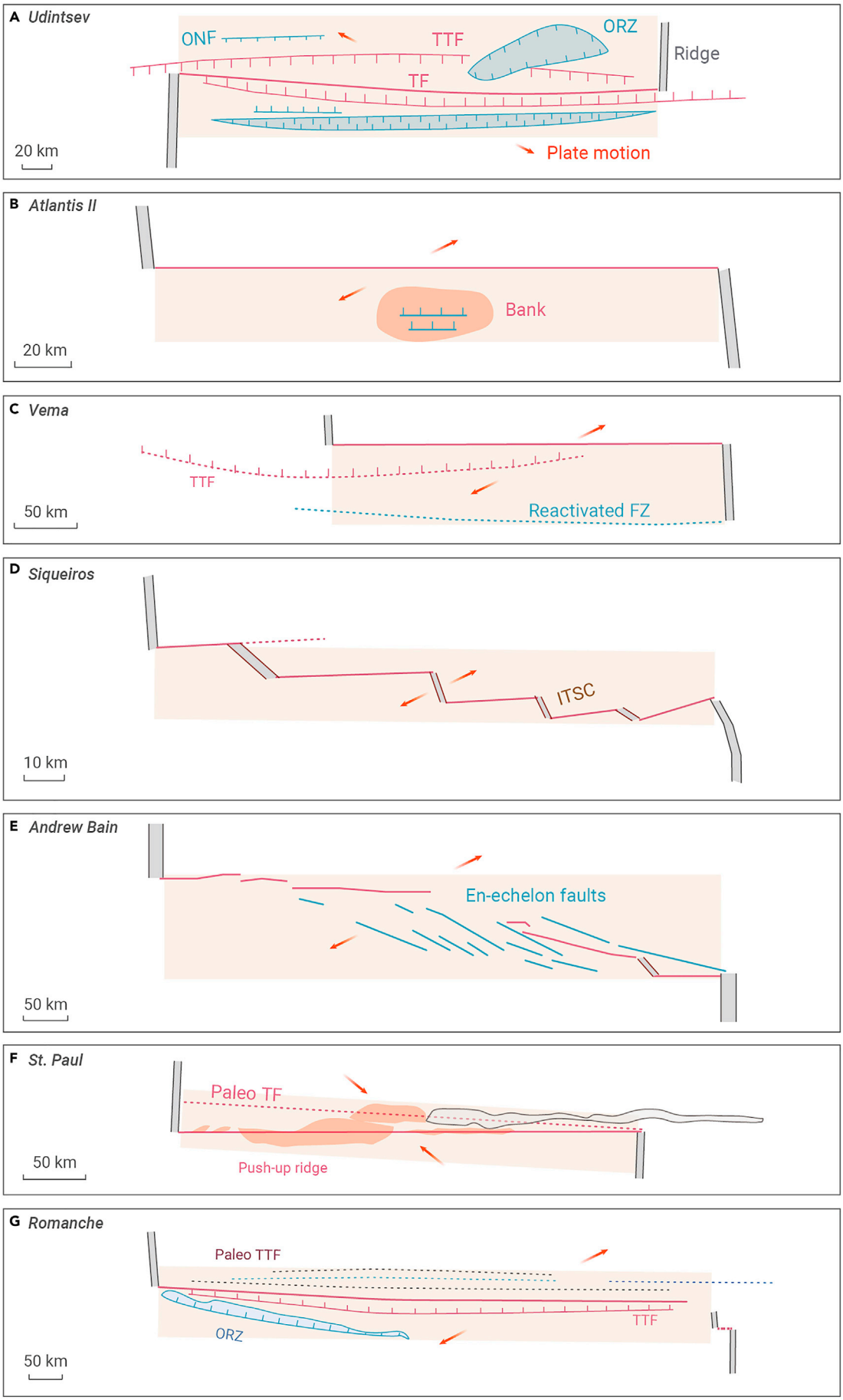

Figure 5. Several distinctive examples[1,4,5,12,18,31–36] of complex deformation on broad zones (light yellow areas) along global oceanic transform faults (A) Udintsev. (B) Atlantis II. (C) Vema. (D) Siqueiros. (E) Andrew Bain. (F) St. Paul. (G) Romanche.

An ORZ may evolve into a new transform plate boundary

An ORZ is also observed along the Romanche ridge-transform system at the slow-spreading MAR, which is more complex (Figure 5G) than the previous examples discussed. In it, two transform valleys, three elongated uplift ridges, and an ORZ are all observed. The TF migrated from north to south at ~8–10 Ma, while the southern valley has remained active.[41] The ORZ south of the active transform boundary ceased activity at ~8 Ma.[28] The Romanche principal transform boundary also migrated from the northern to the southern valley.[41,42] Comparing this behavior with that of the Tharp system, in which an ORZ cuts through the whole length of the TF (Figure 1), we speculate that the active transform valley at the Romanche system could have previously been an ORZ (Figure 5G). We further propose that when mega TFs are too cold and thick to easily rotate in response to a change in the relative plate motion, an ORZ of sufficiently great length may become the new site where a future neighboring TF could be initiated to accommodate the new spreading direction (stage 4; Figure 4E). This may also be the mechanism that has led to the replacement of one or two large-offset transforms with a local system of transforms with the same-sense but smaller offset within the Mendocino and Murray fracture zones, a well-known event that occurred between ~53 and 49 Ma during the evolution of the Northeast Pacific-Farallon Ridge.[43]

MATERIAL AND METHODS

Across-transform deformation and earthquake analysis

The calculated non-Airy-isostatic topography (see supplemental information) should reflect local stress-supported topography.[44] We extracted a series of profiles showing the topography and non-Airy-isostatic topography perpendicular to the Heezen and Tharp TFs (Figure S2). The spacing between two adjacent profiles is 5 km, and the length of each profile is 120 km. Every 10 profiles were grouped as a section, yielding a total of 9, 11, and 2 sections for the Heezen, Tharp, and Pitman TFs, respectively (Figure S2). Using these, we measured the accumulated width and height of the transform uplift, as well as the width and depth of the transform valley, from which we calculated the fault heave (Δx_t) and throw (Δy_t) of each TTF. We also measured the accumulated fault heave (Δx_r) and throw (Δy_r) of each ORZ at the Heezen, Tharp, and Pitman systems. Furthermore, we analyzed the focal mechanisms of $Mw \geq 4.8$ earthquakes from 1976 to 2020 using the global CMT database (globalcmt.org), and calculated the average strike, rake, and dip as well as the accumulated seismic moment of the earthquakes along the Heezen and Tharp systems.

Calculation of stresses required for TTF, ONF, and ORZ

The deviatoric extensional stress ($\Delta\sigma_{xx}$) required to deform a normal fault is given by $\Delta\sigma_{xx} = \frac{2\mu(\rho_c-\rho_w)gy+\tau_0}{\sin 2\theta+\mu(1+\cos 2\theta)}$),[45] where μ is the coefficient of static friction, ρ_c is the rock density of 2,900 kg/m^3, ρ_w is the water density of 1,000 kg/m^3, g is the gravity acceleration of 9.8 m/s^2, y is the depth, τ_0 is the rock cohesion, and θ is the complementary angle to the fault dip angle β. We assume a high dip angle for a TTF (β_t = 75°) and a moderate dip angle for an ONF/ORZ (β_o = 45°), a low friction coefficient of μ_t = 0.1 for a TTF[21,22] and a normal friction coefficient of μ_o = 0.6 for an ONF/ORZ, τ_0 = 0 MPa for a TTF, and τ_0 = 20 MPa for an ONF/ORZ. As plate extension initiates, the TTF will break first due to its negligible cohesion (Figure 2B). When the deviatoric extensional stress rises to become larger than the local rock cohesion, the ONF will start to break, while the TTF will continue to extend (Figure 2C). When deviatoric extensional stresses are large enough, the plate will become totally broken and form an ORZ (Figure 2D).

REFERENCES

1. Bonatti, E., Brunelli, D., Buck, R., et al. (2005). Flexural uplift of a lithospheric slab near the Vema transform (Central Atlantic): timing and mechanisms. Earth Planet. Sci. Lett. ***240***, 642–655.
2. Hekinian, R., Juteau, T., Gràcia, E., et al. (2000). Submersible observations of equatorial atlantic mantle: the St. Paul Fracture Zone region. Mar. Geophys. Res. ***21***, 529–560.
3. Maia, M. (2019). Topographic and morphologic evidences of deformation at oceanic transform faults: far-field and local-field stresses. In Chapter 3 – Transform Plate Boundaries and Fracture Zones (Elsevier), pp. 61–87.
4. Maia, M., Sichel, S., Briais, A., et al. (2016). Extreme mantle uplift and exhumation along a transpressive transform fault. Nat. Geosci. ***9***, 619–623.
5. Menard, H.W., and Atwater, T. (1968). Changes in direction of sea floor spreading. Nature ***219***, 463–467.
6. Pockalny, R.A., Gente, P., and Buck, R. (1996). Oceanic transverse ridges: a flexural response to fracture-zone-normal extension. Geology ***24***, 71–74.
7. Cande, S.C., Raymond, C.A., Stock, J., and Haxby, W.F. (1995). Geophysics of the Pitman Fracture Zone and Pacific-Antarctic plate motions during the Cenozoic. Science ***270***, 947–953.
8. Croon, M.B., and Cande, S.C. (2008). Revised Pacific-Antarctic plate motions and geophysics of the Menard Fracture Zone. Geochem. Geophys. Geosyst. ***9***, Q07001.
9. Wolfson-Schwehr, M., and Boettcher, M.S. (2019). Global Characteristics of Oceanic Transform Fault Structure and Seismicity: Transform Plate Boundaries and Fracture Zones Ch. 2 (Elsevier), pp. 21–59.
10. Boettcher, M.S., and Jordan, T.H. (2004). Earthquake scaling relations for mid-ocean ridge transform faults. J. Geophys. Res. ***109***, 221–232.
11. Müller, R.D., Sdrolias, M., Gaina, C., and Roest, W.R. (2008). Age, spreading rates, and spreading asymmetry of the world's ocean crust. Geochem. Geophys. Geosyst. ***9***, Q04006.
12. Géli, L., Bougault, H., Aslanian, D., et al. (1997). Evolution of the Pacific-Antarctic Ridge south of the Udintsev Fracture Zone. Science ***278***, 1281–1284.
13. Lodolo, E., Coren, F., and Ben-Avraham, Z. (2013). How do long-offset oceanic transforms adapt to plate motion changes? The example of the Western Pacific-Antarctic Plate boundary. J. Geophys. Res. ***118***, 1195–1202.
14. Luo, Y., Lin, J., Zhang, F., and Wei, M. (2021). Spreading rate dependence in morphological characteristics of global transform faults. Acta Oceanol. Sin. ***40***, 39–64.
15. Grevemeyer, I., Rüpke, L.H., Morgan, J.P., et al. (2021). Extensional tectonics and two-stage crustal accretion at oceanic transform faults. Nature ***591***, 402–407.
16. Abrams, L.J. (1986). Morphology and crustal structure of the Kane Fracture Zone transverse ridge. J. Geophys. Res. ***93***, 3195–3210.
17. Tamsett, D., and Searle, R. (1990). Structure of the Alula Fartak Fracture Zone, Gulf of Aden. J. Geophys. Res. ***95***, 1239–1254.
18. Lonsdale, P. (1994). Structural geomorphology of the Eltanin fault system and adjacent transform faults of the Pacific-Antarctic plate boundary. Mar. Geophys. Res. ***16***, 105–143.
19. Lonsdale, P. (1986). Tectonic and magematic ridges in the Eltanin fault system, South Pacific. Mar. Geophys. Res. ***8***, 203–242.
20. Kogan, L.I., Gol'mshtok, A.Y., Zonenshayn, L.P., and Sorokhtin, O.G. (1985). The structure of the Heezen fault in the southeastern Pacific Ocean (Based on deep seismic reflection sounding). Int. Geol. Rev. ***27***, 61–67.
21. Behn, M.D., Lin, J., and Zuber, M.T. (2002). Evidence for weak oceanic transform faults. J. Geophys. Res. ***60***, 1–4.
22. Zoback, M.D., and Beroza, G.C. (1993). Evidence for near-frictionless faulting in the 1989 (M 6.9) Loma Prieta, California, earthquake and its aftershocks. Geology ***21***, 181–185.
23. King, G.C., Stein, R.S., and Rundle, J.B. (1988). The growth of geological structures by repeated earthquakes 1. Conceptual framework. J. Geophys. Res. ***93***, 13307–13318.
24. Zoback, M.D., Zoback, M.L., Mount, V.S., et al. (1987). New evidence on the state of stress of the San Andreas Fault system. Science ***238***, 1105–1111.
25. Croon, M.B., Cande, S.C., and Stock, J.M. (2010). Abyssal hill deflections at Pacific-Antarctic ridge-transform intersections. Geochem. Geophys. Geosyst. ***11***, Q11004.
26. Okal, E.A., and Langenhorst, A.R. (2000). Seismic properties of the Eltanin transform system, South Pacific. Phys. Earth Planet. Inter. ***119***, 185–208.
27. Sykes, L.R., and Ekström, G. (2012). Earthquakes along Eltanin transform system, SE Pacific Ocean: fault segments characterized by strong and poor seismic coupling and implications for long-term earthquake prediction. Geophys. J. Int. ***188***, 421–434.
28. Buck, W.R. (1993). Effect of lithospheric thickness on the formation of high- and low-angle normal faults. Geology ***21***, 933–936.
29. Collettini, C., Niemeijer, A., Viti, C., et al. (2009). Fault zone fabric and fault weakness. Nature ***462***, 907–910.
30. Morrow, T.A., Mittelstaedt, E., and Kim, S.-S. (2019). Are segmented fracture zones weak? Analytical and numerical models constrain anomalous bathymetry at the Clarion and Murray Fracture Zones. Earth Planet. Sci. Lett. ***512***, 214–226.
31. Baines, A.G., Cheadle, M.J., Dick, H.J.B., et al. (2003). Mechanism for generating the anomalous uplift of oceanic core complexes: Atlantis Bank, Southwest Indian Ridge. Geology ***31***, 1105–1108.
32. Bonatti, E. (1978). Vertical tectonism in oceanic fracture zones. Earth Planet. Sci. Lett. ***37***, 369–379.
33. Mathilde, C., and Seyler, M. (1991). Transform tectonics, metamorphic plagioclase and amphibolitization in ultramafic rocks of the Vema transform fault (Atlantic Ocean). Earth Planet. Sci. Lett. ***133***, 283–298.
34. Gasperini, L., Bonatti, E., Borsetti, A.M., et al. (2017). Timing of transverse ridge uplift along the Vema transform (central Atlantic). Mar. Geol. ***385***, 228–232.
35. Gregg, P.M., Lin, J., Behn, M.D., and Montesi, L.G.J. (2007). Spreading rate dependence of gravity anomalies along oceanic transform faults. Nature ***448***, 183–188.
36. Sclater, J.G., Grindlay, N.R., Madsen, J.A., and Rommevaux-Jestin, C. (2013). Tectonic interpretation of the Andrew Bain transform fault: Southwest Indian Ocean. Geochem. Geophys. Geosyst. ***6***, Q09K10.
37. Bird, R.T., Naar, D.F., Larson, R.L., et al. (1998). Plate tectonic reconstructions of the Juan Fernandez microplate: transformation from internal shear to rigid rotation. J. Geophys. Res. ***103***, 7049–7067.
38. Herron, E.M. (1972). Two small crustal plates in the south Pacific near Easter Island. Nature ***240***, 35–37.
39. Li, S., Suo, Y., Li, X., et al. (2018). Microplate tectonics: new insights from micro-blocks in the global oceans, continental margins and deep mantle. Earth Sci. Rev. ***185***, 1029–1064.
40. Lonsdale, P. (1988). Structural pattern of the Galapagos microplate and evolution of the Galapagos triple junctions. J. Geophys. Res. ***93***, 13551–13574.

41. Ligi, M., Bonatti, E., Gasperini, A.N., and Poliakov, L. (2002). Oceanic broad multifault transform plate boundaries. Geology ***30***, 11–14.
42. Bonatti, E., Ligi, M., Gasperini, L., et al. (1994). Transform migration and vertical tectonics at the Romanche Fracture Zone, equatorial Atlantic. J. Geophys. Res. ***99***, 21779–21802.
43. Hey, R.N., Menard, H.W., Atwater, T.M., and Caress, D.W. (1988). Changes in direction of seafloor spreading revisited. J. Geophys. Res. ***93***, 2803–2811.
44. Zhang, F., Lin, J., and Zhan, W. (2014). Variations in oceanic plate bending along the Mariana trench. Earth Planet. Sci. Lett. ***401***, 206–214.
45. Turcotte, D., and Schubert, G. (2014). Geodynamics, Third edition (Cambridge University Press), p. 456.

ACKNOWLEDGMENTS

We benefited from discussions with Drs. Tao Zhang, Huihui Weng, Yen Joe Tan, the SCSIO Deep Ocean Geodynamics Group, the CUHK Seismology Group, and the participants of the InterRidge transform fault workshop in France, 2018. This work was supported by the Southern Marine Science and Engineering Guangdong Laboratory (Guangzhou) (GML2019ZD0205), NSFC grants (41976064, 41890813, 41976066, 91628301, and 91858207), CAS grants (Y4SL021001, QYZDY-SSW-DQC005, 133244KYSB20180029, 131551KYSB20200021, and ISEE2021PY03), National Key R&D Program of China grants (2018YFC0309800 and 2018YFC0310105), the Guangdong Basic and Applied Basic Research Foundation (2021A1515012227), and Hong Kong Research Grant Council grants (14304820 and 14306119).

AUTHOR CONTRIBUTIONS

F.Z. and J.L. conceived and co-wrote the manuscript. F.Z., J.L., and Z.Z. contributed to the data analysis and interpretation. All authors contributed to discussion as well as finalizing and editing the manuscript.

DECLARATION OF INTERESTS

The authors declare no competing interests.

SUPPLEMENTAL INFORMATION

Supplemental information can be found online at https://doi.org/10.1016/j.xinn.2021.100193.

LEAD CONTACT WEBSITE

The contact website for Fan Zhang is at http://www.omg.scsio.ac.cn/document.action?docid=60036 and that for Jian Lin is at https://www2.whoi.edu/staff/jlin/.